Effects of Intracranial Trochlear Neurectomy on the Structure of the Primate Superior Oblique Muscle

Joseph L. Demer,[1,2,3,4] *Vadims Poukens,*[1] *Howard Ying,*[5] *Xiaoyan Shan,*[6] *Jing Tian,*[6] *and David S. Zee*[5,6]

Purpose. Although cyclovertical strabismus in humans is frequently attributed to superior oblique (SO) palsy, anatomic effects of SO denervation have not been studied. Magnetic resonance imaging (MRI) and orbital histology was used to study the effects of acute trochlear (CN4) denervation on the monkey SO.

Methods. Five juvenile macaque monkeys were perfused with formalin for 5 weeks: 15 months after unilateral or bilateral 10-mm intracranial trochlear neurectomy. Denervated and fellow orbits were imaged by MRI, embedded whole in paraffin, serially sectioned at 10-μm thickness, and stained with Masson trichrome. Whole muscle and individual fiber cross sections were quantified in SO muscles throughout the orbit and traced larger fibers in one specimen where they were present.

Results. MRI demonstrated marked reduction in midorbital cross section in denervated SO muscles, with anterior shift of SO mass preserving overall volume. Muscle fibers exhibited variable atrophy along their lengths. Denervated orbital layer (OL) fiber cross sections were slightly but significantly reduced from control at most anteroposterior locations, but this reduction was much more profound in global layer (GL) fibers. Intraorbital and intramuscular CN4 were uniformly fibrotic. In one animal, there were scattered clusters of markedly hypertrophic GL fibers that exhibited only sparse myomyous junctions only anteriorly.

Conclusions. CN4 denervation produces predominantly SO GL atrophy with relative OL sparing. Overall midorbital SO atrophy was evident by MRI as early as 5 weeks after denervation, as denervated SO volume shifted anteriorly. Occasional GL fiber hypertrophy suggests that at least some SO fibers extend essentially the full muscle length after trochlear neurectomy. (*Invest Ophthalmol Vis Sci.* 2010;51:3485–3493) DOI:10.1167/iovs.09-5120

Superior oblique (SO) palsy is prototypic for cyclovertical strabismus. Theoretical, experimental, and much clinical evidence support the idea that acute, unilateral SO palsy produces a small ipsilateral hypertropia that increases with contralateral gaze and with head tilt to the ipsilateral shoulder.[1,2] The basis of this three-step test is traditionally believed to be related to ocular counterrolling, so that the eye ipsilateral to head tilt is normally intorted by the SO and superior rectus (SR) muscles whose vertical actions cancel.[3] However, ipsilateral to a palsied SO, unopposed SR elevating action is supposed to create hypertropia. The three-step test has been the cornerstone of diagnosis and classification of cyclovertical strabismus for generations of clinicians.[4,5] When the three-step test result is positive, clinicians infer SO weakness and attribute the large amount of interindividual alignment variability to secondary changes,[6] such as inferior oblique overaction and SR contracture. Much evidence, however, indicates that the mechanism of the three-step test is misunderstood. If traditional teaching were true, then IO weakening, the most common surgery for SO palsy, should increase the head tilt-dependent change in hypertropia; the opposite has been observed.[7] Among numerous inconsistencies with common clinical observations,[7] bilateral SO palsy should cause greater head-tilt-dependent change in hypertropia than should unilateral SO palsy; however, the opposite has been found.[8,9] Modeling and simulation of putative effects of head tilt in SO palsy suggest that SO weakness alone cannot account for typical findings in the three-step test.[10,11] Beyond actual contractile weakness of the SO muscle, additional changes in other extraocular muscles (EOMs) have been typically postulated in SO palsy.

Functional anatomic studies had added some insight into cases of hypertropia such as SO palsy. High-resolution magnetic resonance imaging (MRI) has quantified normal changes in SO cross sections with vertical gaze, and, in at least some cases, SO atrophy and loss of gaze-related contractility are associated with SO palsy.[12–15] However, MRI findings have not consistently supported the clinical diagnosis of SO palsy. A striking anomaly has been the nonspecificity of the three-step test for structural abnormalities of the SO belly, tendon, and trochlea, found only in ~50% of patients by MRI.[16] Even in patients selected because MRI demonstrated profound SO atrophy, there was no correlation between clinical motility and inferior oblique size or contractility.[15] Multiple conditions can simulate the SO palsy pattern of incomitant hypertropia.[17] Vestibular lesions produce head-tilt-dependent hypertropia, also known as skew deviation,[18] that can mimic SO palsy by the three-step test.[19] Pulley heterotopy can simulate SO palsy[20] but is probably not its result, since SO atrophy is not associated with significant alterations in pulley position in central gaze.[21] Overall, clinical alignment findings are not specific for SO palsy, but the possibility that functional imaging of the SO could be specific for SO palsy remains to be established.

A primate model of SO palsy avoids potentially confounding conditions and has permitted detailed study of the evolution of ocular motor findings.[22–27] In the rhesus macaque monkey, trained to fixate, and chronically implanted for binocular, three-dimensional eye movement recording, intracranial trochlear neurectomy (ITN) produces an ipsilateral hypertropia and excyclotropia that is maximum in the SO field of action and is associ-

From the Departments of [1]Ophthalmology, Jules Stein Eye Institute, [2]Neurology, the [3]Bioengineering Interdepartmental Program, and the [4]Neuroscience Interdepartmental Program, University of California Los Angeles, Los Angeles, California; and the Departments of [5]Ophthalmology and [6]Neurology, The Johns Hopkins Medical School, The Johns Hopkins University, Baltimore, Maryland.

Supported by Grants EY01849, EY019347, EY08313, EY00331, and DC005211 from the U.S. Public Health Service and by Research to Prevent Blindness. JLD is the Leonard Apt Professor of Ophthalmology. Jing Tian is a Betty and Paul Cinquegrana scholar.

Submitted for publication December 23, 2009; revised January 27, 2010; accepted January 28, 2010.

Disclosure: **J.L. Demer**, None; **V. Poukens**, None; **H. Ying**, None; **X. Shan**, None; **J. Tian**, None; **D.S. Zee**, None

Corresponding author: Joseph L. Demer, Jules Stein Eye Institute, 100 Stein Plaza, UCLA, Los Angeles, CA 90095-7002; jld@ucla.edu.

TABLE 1. Procedures and Survival

Monkey	Laterality of ITN	Survival (wk Since Lesion)	Further Procedures
M1	Left	59	IO denervation and extirpation 6 mo later
M2	Right	65	IO denervation and extirpation 4 mo later
M3	Right	5	None
M4	Right and left	5 and 10	Left trigeminal (V1–3) section with left ITN
M5	Left	74	Concurrent left V3 section

ated with ipsilesionally impaired torsional optokinetic nystagmus,[25] and downward saccades,[23] and pursuit.[24] These findings are consistent with classic concepts of SO action, but the evolution of the ipsilesional hypertropia over time after lesion suggests contributions from other factors, including adaptive mechanisms and proprioception.[22] Obviously denervation-related structural changes in the SO itself would be important. Computational modeling of these findings can help generalize the understanding of secondary changes associated with SO palsy.[27]

After completion of behavioral studies in monkeys with ITN, their cadaveric specimens have become available for detailed anatomic analysis. We sought to determine the MRI features of SO palsy and to correlate them with quantitative histology.

METHODS

Subjects

Adult monkeys M1 and M2 had undergone detailed behavioral ocular motor evaluations before and after unilateral removal of a 10-mm segment of the subarachnoid trochlear nerve (ITN).[22–26] In M1 and M2, ITN was followed 4 to 6 months later by denervation and extirpation of the ipsilateral IO muscle, with death 56 to 74 weeks after ITN (Table 1). Animals M3 and M4 did not undergo detailed behavioral studies after ITN. Animal M3 was killed 5 weeks after right ITN. Monkey M4 underwent sequential bilateral ITN, on the left side 10 weeks and on the right side 5 weeks before death, with section of all divisions of the left trigeminal nerve 10 weeks before death. Monkey M5 underwent concurrent right ITN and sectioning of the mandibular division of the trigeminal nerve (V3) 6 weeks before death. Several of the monkeys also had small cerebellar lesions in the nodulus and uvula as part of a separate behavioral experimental protocol. As described, animals were humanely euthanatized and perfused intrarterially with 10% neutral buffered formalin.[22] All animal use was in compliance with the ARVO Statement for the Use of Animals in Ophthalmic and Vision Research; protocols were approved by the Johns Hopkins University Animal Care and Use Committee.

Magnetic Resonance Imaging

After removal of the brains, all implanted hardware was carefully removed by dissection under magnification. The mandible and muscles of mastication were removed to reduce specimen size without disturbing the orbits. Specimens were warmed to approximately 37°C in hot water and placed in plastic bags for MRI. Dual 10-cm diameter, phased-array surface coils (General Electric, Milwaukee, WI) were placed on opposite sides of each specimen with the centers of the surface coils as close as possible to the orbits. The orbits were imaged with a 1.5-T scanner (Signa; General Electric) using T_1-weighted pulse sequence in the axial plane, quasi-coronal planes perpendicular to the long axis of each orbit, and quasi-sagittal planes parallel to the long axis of each orbit. Image planes were 1.5- to 2.0-mm thick with a field of view of 4 to 6 cm and matrix of 256 × 256, providing an in-plane resolution of 156 to 234 μm. To improve signal to noise ratio, each acquisition included 6 to 10 excitations. Cross sections of the SO were outlined in MRI scans using the digital cursor of the program ImageJ (NIH Image or ImageJ software developed by Wayne Rasband, National Institutes of Health, Bethesda, MD; available at http://rsb.info.nih.gov/ij/index.html) for quantitative analysis.

Histologic Imaging

After MRI, each orbit was removed en bloc with the periorbita intact. Orbital bones were removed using rongeurs and a high-speed bone

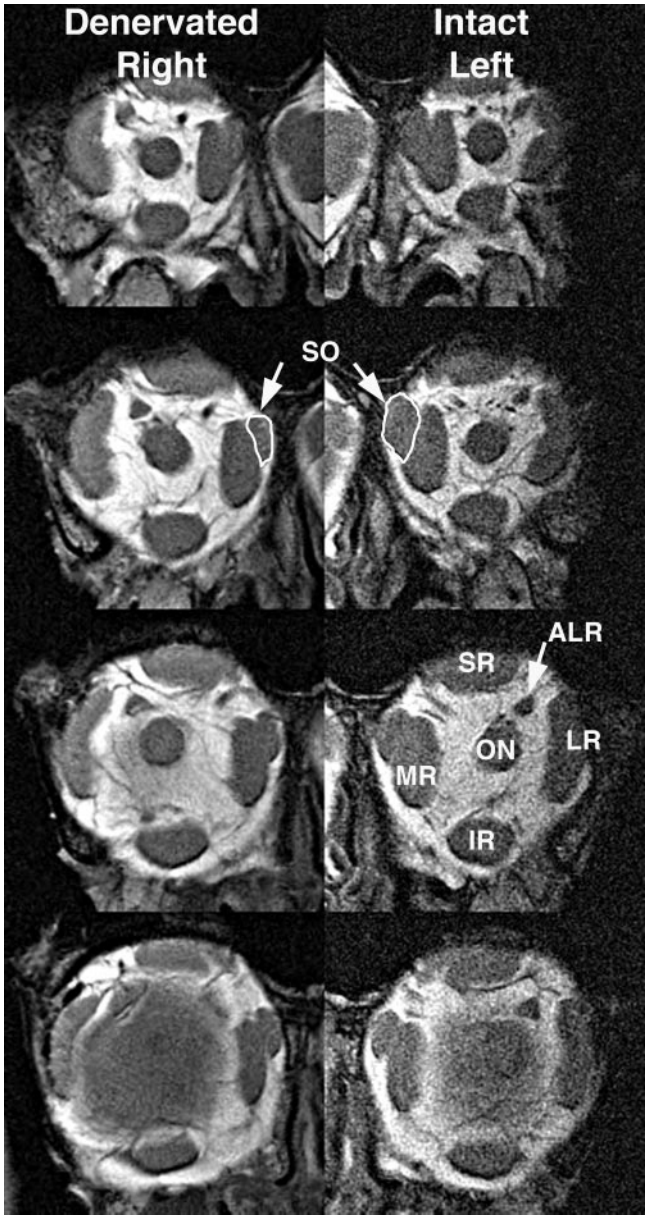

FIGURE 1. MRI of both orbits of monkey M2 in 2-mm-thick quasi-coronal planes spaced at 4-mm intervals from posterior (*top*) to anterior (*bottom*). Note smaller SO muscle (*white outline*) in the deep orbit on the right side denervated by ITN. ALR, accessory lateral rectus muscle; IR, inferior rectus muscle; LR, lateral rectus muscle; MR, medial rectus muscle; ON, optic nerve; SO, superior oblique muscle; SR, superior rectus muscle.

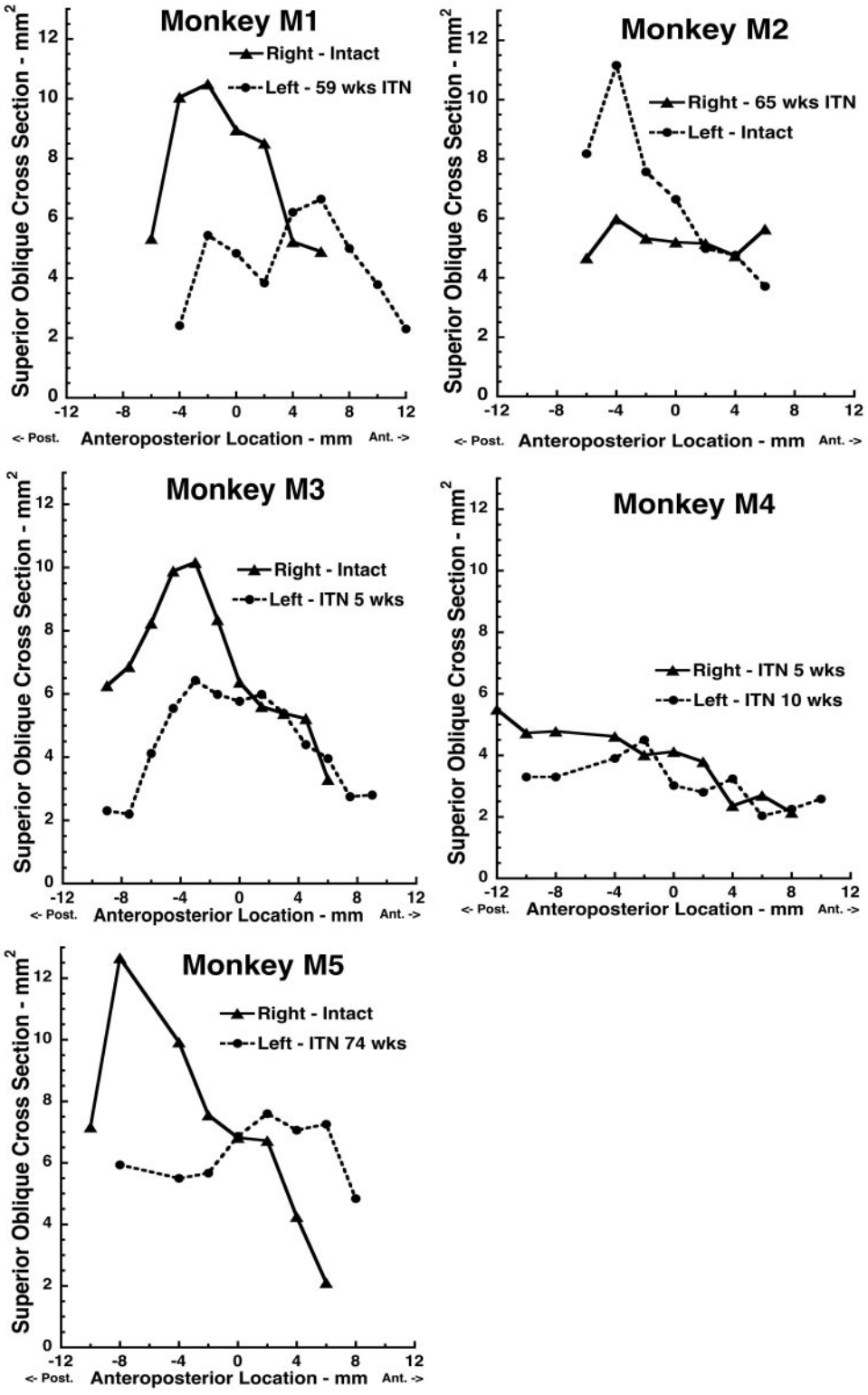

FIGURE 2. MRI determinations of SO cross sections in monkeys M1 to M5 as functions of anteroposterior location relative to the junction of the globe with the optic nerve, designated as 0. All denervated SO muscles exhibited reduced cross-sectional area posterior to the globe.

drill. Bone near the trochlea was carefully removed by dissection under magnification. As previously described, the whole orbits were sectioned in the quasi-coronal plane into 10-μm-thick sections by a microtome (HM325; Carl-Zeiss, Thornwood, NY) after tissue processing, including formalin fixation, decalcification, dehydration in alcohol and xylenes, and embedding in paraffin.[28–31] Processing was identical in all specimens and resulted in approximately 3000 sections per orbit, of which approximately every 10th was stained with Masson trichrome stain to distinguish collagen (blue), muscle (red), and nerve (purple).[32] The cavernous sinuses were isolated individually and sectioned transversely in monkey M5. Stained sections were digitally photographed at 1× to 100× magnification (Eclipse microscope; Nikon, Melville, NY).

Cross sections of the SO were outlined from digital photomicrographs with ImageJ. Selected individual fibers in the orbital (OL) and global layer (GL) were also outlined in mid-orbital sections for cross section analysis. In monkey M2, a bundle of 14 hypertrophic fibers was selected in mid orbit and the distinctive fibers were individually num-

bered and traced in micrographs posteriorly to the SO origin, and anteriorly to the transition to tendon.

Results

Magnetic Resonance Imaging

A coronal plane MRI in the deep orbit, comparable to what would typically be available clinically in humans, demonstrated that all denervated SO EOMs had smaller cross sections than did innervated SO EOMs (Fig. 1). This reduction was evident posterior to the globe–optic nerve junction, but did not affect the anterior tendon region, which had a cross section that was either slightly increased (Fig. 2 M1 and M5) or unchanged ipsilateral to the ITN compared with that on the intact side (Fig. 2 M2 and M3).

Qualitative impressions of the effect of ITN on SO cross section were confirmed by quantitative analysis of posterior cross sections in all coronal MRI planes in which the SO cross section was sufficiently distinguishable that it could be reliably outlined (Fig. 2). In every case of unilateral ITN, the cross section of the denervated SO in every image plane posterior to the globe–optic nerve junction was less than that of the innervated SO. In monkey M4 who had undergone bilateral ITN, the SO cross section was low bilaterally, comparable to that of the denervated SO in the other animals. There was no systematic variation with duration of ITN.

Histologic Imaging

Analysis of histologic sections taken in the same planes as the MRI scans confirmed the findings of loss of the overall cross section of the deep SO belly. This loss is evident in Figure 3, which shows a smaller left SO cross section at the globe–optic nerve junction of monkey M1, 56 weeks after ITN. Note that this atrophy could not be the result of a variation in vertical eye position, since the globe–optic nerve junction on the denervated left side is superior to that on the intact right side, implying that the left eye was more infraducted than the right. In an infraducted position where the SO is normally contracted, SO volume would normally shift posteriorly.

Quantitative analysis of SO cross sections throughout the length of the orbit from SO origin to the trochlea permitted determination of total gross SO volume in monkeys M1, M2, and M3. This determination did not consider the effects of microscopic voids among EOM fibers, which probably represent shrinkage artifacts. Despite the 40% to 50% reduction in deep SO cross section after ITN evident in Figure 2, the effect of ITN on SO volume was smaller and inconsistent (Fig. 4).

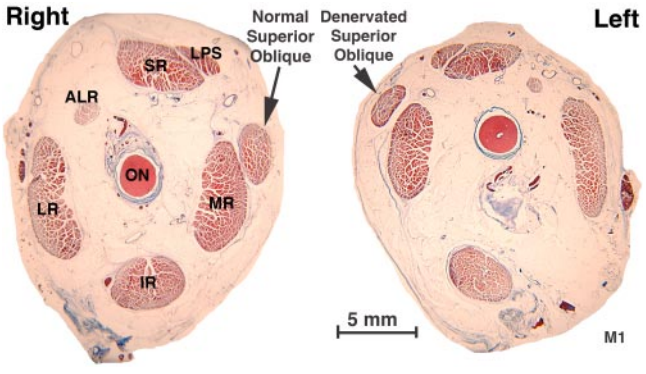

Figure 3. Coronal histologic sections of the right and left orbits of monkey M1, 56 weeks after left ITN, at the globe–optic nerve junction, designated as image plane 0, showing left SO muscle atrophy. Masson trichrome. Abbreviations as in Figure 1.

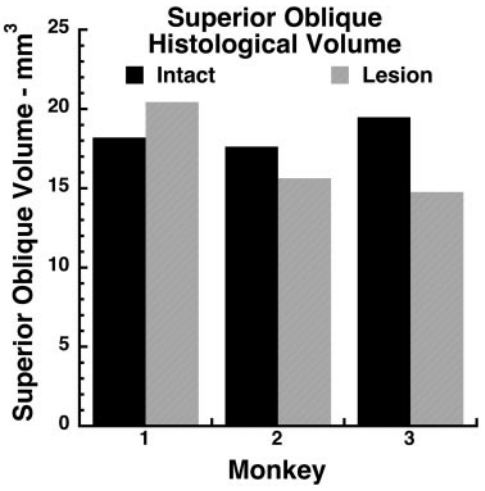

Figure 4. Total gross volumes of SO muscles determined from coronal histologic sections in monkeys M1 to M3 who had undergone unilateral ITN. Note the absence of consistent volume reduction by ITN.

Total SO volume after ITN was 18% greater than on the intact side in M1, but was 12% less in M2 and 26% less in M3.

The minimal or, in the case of M1, paradoxical effect of ITN on SO volume was explained by a large, anterior shift of SO belly mass, even into the trochlea. This shift is described qualitatively in Figure 5, which illustrates coronal histologic sections of the SO 8 mm anterior to the globe–optic nerve junction in monkeys M1, M2, and M3. At this location, the normal SO exhibited transition of GL fibers to the tendon. The OL was absent, having inserted posteriorly on the peripherally located SO sheath that enveloped the SO. In each case of unilateral ITN, the belly of the denervated SO exhibited a larger cross section than did the innervated SO. In monkeys M1 and M2, the OL was also present at this anterior location.

Higher power histologic examination disclosed fibrosis of the entire trochlear nerve, including its intramuscular branches, as evident from the blue staining on Masson trichrome stain. Normal nerves stained purple with Masson trichrome. Normal GL fibers were relatively large and brighter red staining, whereas normal OL fibers are smaller and darker staining (Fig. 6). In every case examined histologically after ITN, the great majority of denervated GL fibers were much smaller and irregularly sized. In the denervated OL, most fibers were slightly smaller than normal, although some approached or exceeded normal size, and were also more irregular.

Quantitative cross section analysis was performed for samples of 50 contiguous representative fibers in the OL and GL along the length of the SO muscles of monkeys M1, M2, M3, and M4. These data, which do not include the small number of giant fibers in monkey M2, are presented in Figure 7. In normally innervated SO muscles, GL fiber cross section averaged 400 to 600 μm^2, and OL fiber cross section averaged 100 to 300 μm^2. After ITN, GL fiber cross section averaged 100 to 300 μm^2, and OL fiber cross section averaged 100 to 250 μm^2. Analysis of variance for both GL and OL cross sections showed a significant effect of lesion ($P < 0.01$), but no significant effects of individual animal or anteroposterior location along the SO. The effect on GL cross section was greater than on the OL.

Monkey M2 exhibited the unique finding of marked hypertrophy of clusters of GL fibers (Fig. 8). In our laboratory, no other giant fibers have been seen in any EOM in similar careful examinations prepared with an identical serial histologic technique, of 10 human orbits, more than 30 monkey orbits, one cow, one rabbit, one horse, and one dog orbit. There was no apparent reason for giant fibers to be present in M2 but not in

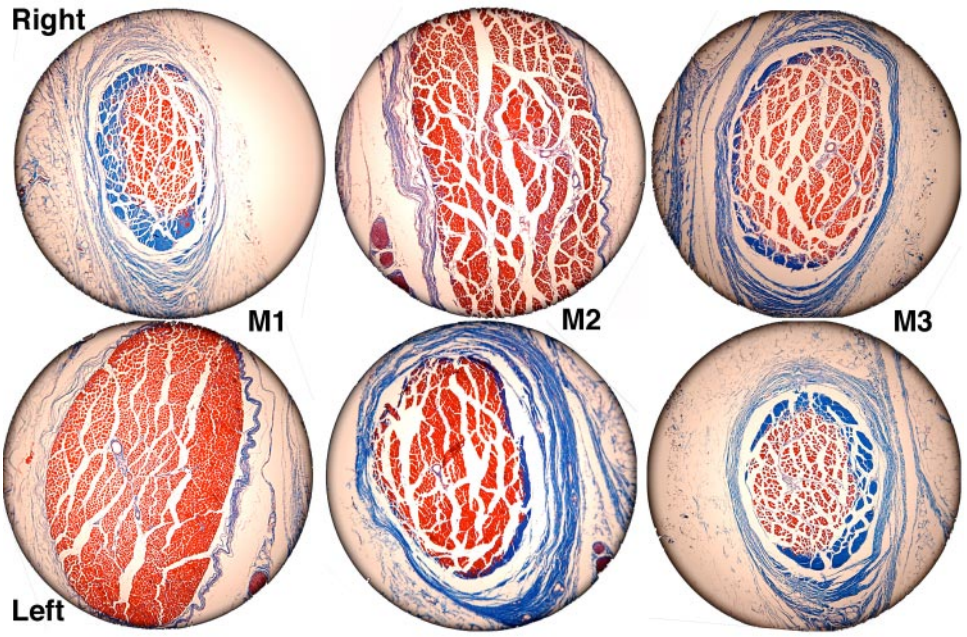

FIGURE 5. Coronal histologic sections of the SO taken 8 mm anterior to the globe–optic nerve junction showing anterior shift of fibers in the denervated left orbit of monkey M1 and the denervated right orbits of monkeys M2 and M3. Masson trichrome. Circular field diameter, 2.2 mm.

the other animals subjected to the same lesion. These giant fiber clusters were typically surrounded by numerous, profoundly atrophic GL fibers. A fiber cross section was analyzed quantitatively in a sample of 100 fibers in and around the giant fibers in a section 2 mm posterior to the globe–optic nerve junction of M2 (Fig. 9). In this sample, the mode of the cross section distribution was 75 μm^2, but giant fibers had cross sections ranging up to 1000 μm^2, so that the mean of the distribution was 158 μm^2. No giant fibers were present in monkey M2's OL, or in the GL or OL of any other animal.

Although the numerous individual GL and OL fibers are too small and too similarly shaped to be traced along their lengths for significant distances, the small number of giant fibers in M2 had large, distinctive cross sections that were suitable for identification and tracing in serial sections. A sample of 14 giant GL fibers in the midorbit of M2 was assigned identification numbers. By comparison with sequential micrographs, the length of each fiber was traced from beginning to end. Divisions or junctions of fibers were given subsidiary identification numbers, and the resulting fiber paths were graphed (Fig. 10). Six fibers extended from origin to tendon without myomyous junction for at least 26 mm, whereas eight fibers exhibited myomyous junctions. These myomyous junctions were uncommon, and were present only in the anterior portions of the EOM.

The cavernous sinuses were transversely sectioned in monkey M5, who had undergone left ITN 74 weeks earlier. Because the cavernous sinus contents were removed from the surrounding bones to permit sectioning, it was difficult to identify specific nerves within it. All nerves in the right cavernous sinus exhibited normal staining and morphology. A nerve in the left cavernous sinus, presumably the trochlear nerve, exhibited marked fibrosis. There was no indication of axon regrowth within or around this nerve.

DISCUSSION

ITN rapidly produced consistent changes in the simian SO muscle. Within 5 weeks of ITN, all five animals in this series exhibited marked reduction in the cross section of the posterior SO belly. This reduction in cross section, which may be considered neurogenic atrophy, was obvious on coronal plane MRI in the region where the SO would be evaluated in a human patient in the diagnostic evaluation of SO palsy. Despite the consistent demonstration of gross neurogenic atrophy of the SO belly after ITN, the present study found some complex subtleties in SO anatomy after this lesion. Gross cross section of the SO muscle was not uniformly reduced along the entire length of the EOM. In fact, the SO cross section was redistributed anteriorly so that the overall SO volume was only minimally reduced or even slightly increased relative to the control specimen (Fig. 4). The fiber cross-sectional area in the denervated SO was decreased, more strikingly in the GL than in the OL, but again variably as sampled throughout the length of the EOM. In a single animal, M2, clusters of giant muscle fibers were present in the GL that appeared to extend nearly the entire length of the SOM, with only a few myomyous junctions limited to the most anterior part of the SO. The trochlear nerve and its intramuscular branches were profoundly fibrotic in all animals, showing no signs of residual or regenerated axons.

The literature is inconsistent regarding the effect of denervation on the EOMs, which in the past have been sampled mainly or exclusively at a single point along their lengths. After denervation in the rabbit, the inferior oblique (IO) muscle is grossly hypertrophic, and the cross sections of several fiber types increase.[33,34] Late postdenervation hypertrophy in rabbit IO was found to be predominantly due to hypertrophy of the OL fibers, offsetting the progressive GL fiber atrophy that follows an initial transient GL fiber hypertrophy.[35] These observations were made at the midbelly of the IO. After oculomotor nerve transection in *Macaca fascicularis* monkeys, Porter et al.[36] found progressive reduction in medial rectus (MR) fiber cross section to 50% of the control by 112 days after oculomotor nerve section, followed by hypertrophy to approximately 50% greater than the control by 6 months, when reinnervation occurred from an unknown, presumably nonoculomotor source. Changes were greatest in OL and GL singly innervated fiber cross sections, but it should again be noted that Porter et al.[36] sampled fiber sizes at only one point near the innervation zone. Oculomotor nerve transection in the dog was associated with a reduction in IO fiber diameter of ~20%, as assessed in biopsies performed 3 months later,[37] and 20% to 30% reduction in MR and inferior rectus (IR) midbelly fiber diameter at time intervals up to 3 months.[38] These reductions

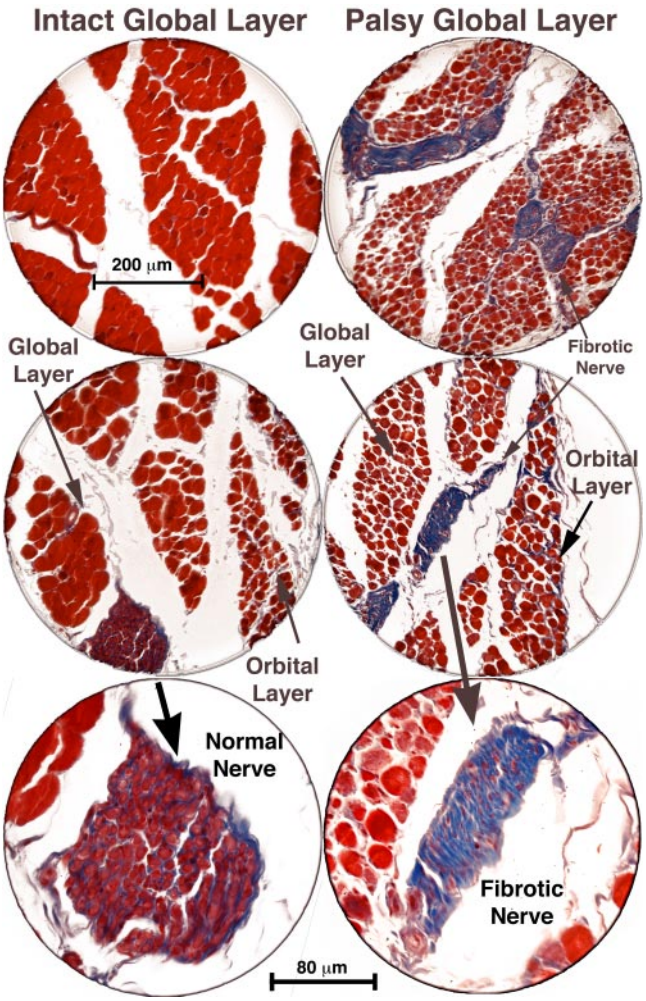

FIGURE 6. Coronal histologic sections of the right and left orbits of monkey M1, 56 weeks after left ITN, showing marked atrophy of global layer fibers in the left SO muscle, with preservation of left orbital layer fibers. Fibrotic intramuscular nerves (shown at higher power in *bottom panels*) in the palsied left SO stain *blue* with Masson trichrome, whereas intact nerves in the right SO stain *purple*. Scale bars: (*top two panels*) 200 μm; (*bottom panel*) 80 μm.

were significant only in canine singly innervated fibers, but were similar in both the OL and GL.

The present study of the denervated monkey SO is most consistent with prior reports of relatively mild denervation atrophy, but our complete analysis of SO cross sections along the length of the EOM may allow reconciliation of seemingly contradictory prior findings. At certain points along the length of the SO belly, cross sections of denervated OL and GL fibers equaled or exceeded those of contralateral innervated fibers (Fig. 7). Sampling of such regions might have suggested the absence of denervation atrophy or even the presence of denervation hypertrophy. The effect of sampling error could also have arisen from biopsy of the less affected OL in early studies that did not distinguish the layers, or from local reinnervation hypertrophy. Nevertheless, the convincing gross hypertrophy of the rabbit IO demonstrated early and long after denervation by Asmussen and Kiessling[33,34] suggests that there might exist species-specific or even individual EOM-specific differences in EOM responses to denervation.

Monkey M2 exhibited the unique finding of clusters of hypertrophic GL fibers that were sufficiently large and morphologically distinctive to be traced for nearly the entire length of the SO. There was no apparent reason for giant fibers to be present in M2 but not in the other animals subjected to the same lesion. The giant fibers did not exhibit prominent myomyous junctions, except to a limited degree at their anterior ends. This finding is in contrast to the report of Harrison et al.[39] in rabbit and monkey superior rectus (SR) that GL fibers average only 24% of overall EOM length. Possible explanations of the difference in findings include a systematic difference between oblique and rectus EOMs, or selective preservation of longer GL fibers after ITN. This question is important, however, since fiber length and interaction via myomyous junctions determines how much of each fiber's tension is transmitted into oculorotary force at the scleral junction.[40,41] Resolution of this question of EOM fiber length requires further studies.

In our laboratory, giant fibers have never been seen in any EOMs in examinations with complete serial sectioning of 10 human orbits, more than 30 monkey orbits, one cow, one rabbit, one horse, and one dog orbit. It therefore seems unlikely that the giant fibers existed before ITN in M2. The giant fibers in M2 most likely resulted from reinnervation, which is known to occur in EOMs with preservation of the characteristic distinction between the OL and GL.[36] However, in the present study there was no reanastomosis of the trochlear nerve, which remained severely fibrotic in all animals. Examination of the cavernous sinus in M5 showed persistent fibrosis of the presumed trochlear nerve, even 74 weeks after ITN, a finding also arguing against trochlear nerve anastomosis. Sparse reinnervation of the relevant EOMs has been demonstrated by the presence of motor endplates, even after apparently complete and permanent interruption of the intracranial oculomotor nerve.[38] This persistent or new innervation may not represent trochlear nerve regeneration, but may instead be autonomic. After transsection of the proximal oculomotor nerve, a classic anatomic study in cat demonstrated autonomic fibers entering the distal oculomotor nerve at the ciliary ganglion and suggested termination of a vascular autonomic nerve on an EOM fiber.[42] Normal fine structure of the rabbit SR is preserved for at least 3 weeks after oculomotor nerve section in the vicinity of unmyelinated, presumably sympathetic, nerve fibers.[43] Although the giant fibers encountered in M2 were often in the vicinity of intramuscular vessels, additional investigations of the possible nontrochlear innervation of the SO are beyond the scope of the present study. From whatever cause, the relative preservation of the denervated SO fibers offers the possible opportunity of therapeutic rescue by later trochlear reinnervation, or some other modality, such as artificial electrical stimulation.[44]

The monkeys whose anatomic findings are reported herein exhibited a complex evolution in strabismus over a period of 30 days, with a nonmonotonic variation in hypertropia over time.[22] Although some of the changes in strabismus might have been due to the mechanical effects of SO fiber atrophy and gross stretching of the SO belly, the present results indicate that gross mechanical changes were complete by 5 weeks after ITN, approximately the duration of the behavioral study. The small number of possibly reinnervated giant fibers in M2 cannot explain similar late alignment changes observed in M1,[22] which never developed giant fibers. It must be concluded that the late changes arose from innervational alterations to other, functional EOMs, not activity of the ipsilesional SO itself. This conclusion is consistent with MRI evidence of compensatory functional anatomic changes in the IR in humans with SO atrophy due to palsy.[45] Widespread changes in innervation to multiple EOMs may explain the absence of relationship between oblique EOM size and magnitude of the head tilt phenomenon in human SO palsy,[46] and the effect of prolonged diagnostic occlusion, which in many humans with longstanding SO palsy causes an increase in excyclotropia without a consistent change in hypertropia.[47] Dissociation between the

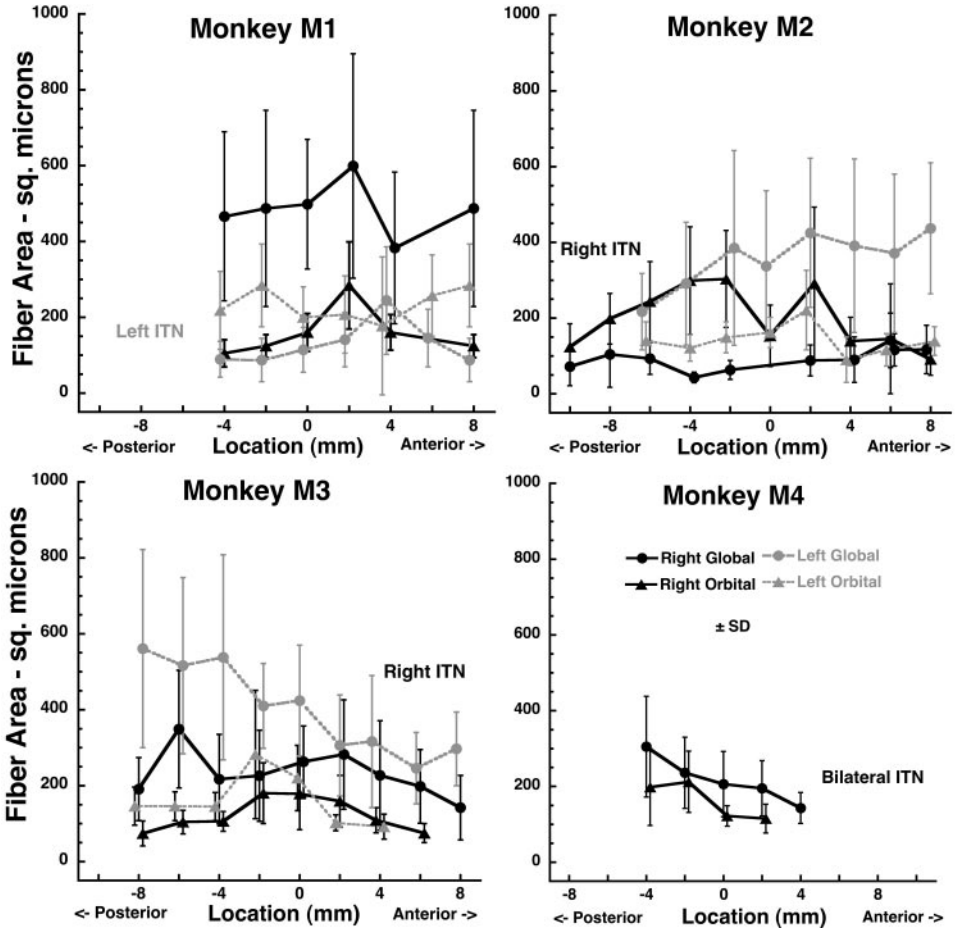

FIGURE 7. Mean cross sectional areas of fibers in the SO GL and OL. Monkey M1 had undergone left ITN, M2 and M3 underwent right ITN, and M4 underwent bilateral ITN, but data are analyzed only for the right side. Note the marked reduction in denervated GL, but not OL fiber cross section. Each data point is the mean of 50 fibers. The abscissa is aligned on the globe–optic nerve junction.

mechanically expected effects of IO action in the setting of SO palsy implies the existence of selectively controllable cyclovertical actions of the rectus EOMs. A mechanism for neural control of cyclovertical action of the LR has recently been suggested based on its compartmentalization into superior and inferior zones.[48]

It has been suggested that proprioception may mediate late changes in binocular alignment after SO palsy.[22] Orbital proprioception is probably mediated by the trigeminal nerve.[49,50] Although the present study did not address the influence of proprioception in detail, bilateral ITN in monkey M4 was supplemented by left-side trigeminal neurectomy, which included ophthalmic division. Morphologic changes in the SO of M4 were nevertheless bilaterally symmetrical and were similar

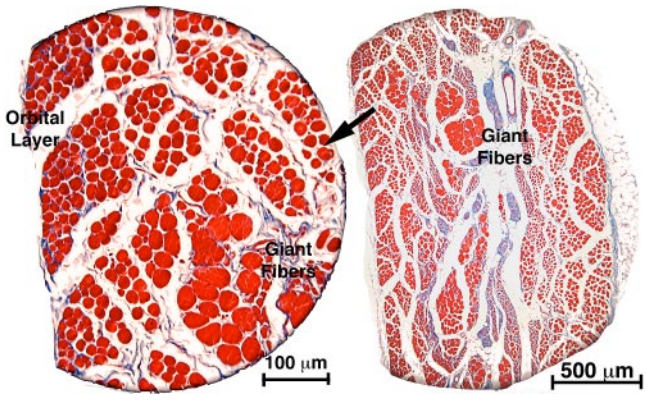

FIGURE 8. Coronal histologic section of the right orbit of monkey M2, 60 weeks after right ITN, showing clusters of giant fibers among the severely atrophic fibers in the GL. Masson trichrome stain. Section taken 2 mm posterior to the globe–optic nerve junction.

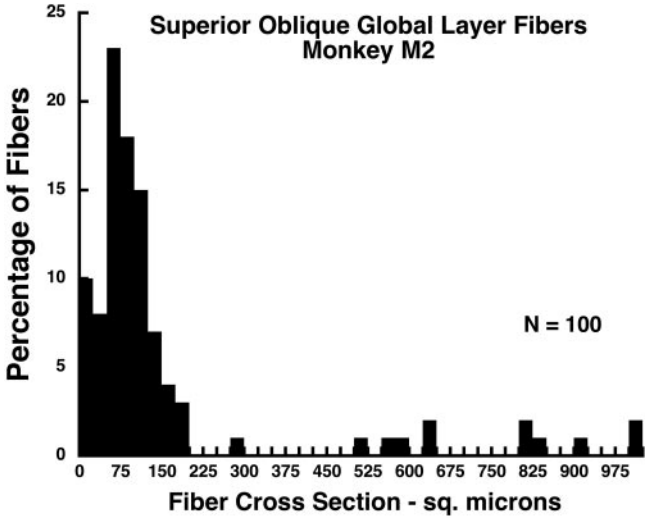

FIGURE 9. Histogram of GL fiber cross sections in the right orbit of monkey M2, 60 weeks after right ITN, showing clusters of giant GL fibers among the severely atrophic fibers in the GL. Mode for atrophic fibers is 75 μm^2, but some hypertropic fibers exhibited cross sections of up to 1000 μm^2 so that the mean for all fibers was 158 μm^2. Section were taken 2 mm posterior to the globe–optic nerve junction and are illustrated in Figure 8.

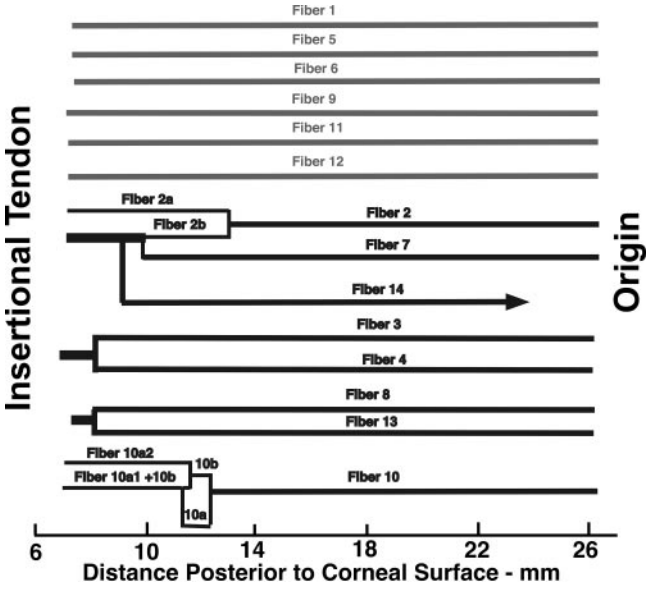

FIGURE 10. Longitudinal tracing of 14 identified giant SO GL fibers in the right orbit of monkey M2 after right ITN. Six fibers extended from origin to tendon without myomyous junctions, whereas eight fibers exhibited anterior myomyous junctions.

to changes observed in the animals not subjected to sensory lesions. This finding suggests that the presence of trigeminal innervation does not significantly alter the effects of ITN on the SO muscle.

The current finding of SO atrophy after ITN confirms in the monkey the human imaging finding that the SO belly is atrophic in SO palsy[12–15,21,45,46,51–55] and extends this finding to SO palsy that is unequivocally acquired in addition to the congenital condition.[13,56,57] On the basis of the present results, it would be anticipated that appropriate orbital MRI in humans would demonstrate neurogenic atrophy of the deep SO belly within 5 weeks of denervation. The fine time scale of this prediction remains to be confirmed in humans.

Despite the consistent demonstration of gross neurogenic atrophy of the SO belly and microscopic atrophy of fibers after ITN, the present study found some complex but clinically relevant subtleties in SO anatomy after this lesion. The overall SO cross section would not correlate perfectly with mean fiber cross section spaces between fibers changed after ITN; such a change in fiber spacing could be subject to local shrinkage artifact. Gross cross section of the SO muscle was not uniformly reduced along the entire length of the EOM. In fact, the SO cross section was redistributed anteriorly so that overall SO volume was only minimally reduced or even slightly increased relative to the control (Fig. 4). The apparent slight increase in SO volume in M1 may reflect a prelesion volume difference or a measurement error. A parsimonious interpretation of these findings would be that after ITN, the SO maintained its volume but was simply stretched to a greater resting length that would be associated with reduced resting passive elastic tension. Such an interpretation is consistent with the report that intraoperative mechanical assessment of SO tendon laxity correlates with atrophy of the SO belly in congenital SO palsy.[56] It therefore appears likely that SO laxity can be the result of acquired SO denervation and is not an exclusively congenital phenomenon. Strabismus surgeries designed to "strengthen" the SO by placating its anterior tendinous portion until excess length is corrected may,[58] in such cases, fail to affect the permanently absent contractile force of a denervated SO muscle. Computational modeling of SO palsy would appropriately set the contractile force to 0, increase the SO resting length, and reduce its stiffness.[59] It is unknown whether these changes would be reversible if the SO became reinnervated by the trochlear nerve. Potentially, even brief, transient SO denervation by a reversible cause such as ischemic mononeuropathy or trauma may lead to permanent SO elongation after 5 weeks or less. Modeling of resolved SO palsy after recovery of trochlear innervation may appropriately set contractile force to normal, but with increased SO resting length and stiffness. Perhaps surgical shortening of the SO tendon would be a logical therapy for hypertropia when the SO muscle has become elongated by transient but ultimately resolved denervation.

Despite the additional anatomic complexity revealed by the present study of ITN, the mechanism of the three-step test in SO palsy remains mysterious. Existing limited evidence continues to support contributions from complex adaptations to ipsilesional SO changes, including increased size and contractility of the contralesional inferior rectus muscle[45] and possibly proprioception.[22]

The complex pattern of changes in the monkey SO muscle that evolve rapidly after ITN highlight the general complexity of EOMs. Appreciation of these changes should be valuable in distinguishing the mechanical effects of denervation changes in the SO muscle from postulated complex, possibly proprioceptive neural adaptations to SO palsy that remain to be elucidated.[22,23,25] To this end, additional anatomic investigations performed with shorter intervals after ITN would provide valuable insight into the rapid structural changes in the SO that follow denervation.

Acknowledgments

The authors thank David Ryugo for performing the perfusions and Corena Bridges, Dale Roberts, John Ghazaryan, and Adrian Lasker for technical support.

References

1. Bielschowsky A. Lectures on motor anomalies. XI. Etiology, prognosis, and treatment of ocular paralyses. *Am J Ophthalmol.* 1939; 22:723–734.
2. von Noorden GK, Murray E, Wong SY. Superior oblique paralysis: a review of 270 cases. *Arch Ophthalmol.* 1986;104:1771–1776.
3. Adler FE. Physiologic factors in differential diagnosis of paralysis of superior rectus and superior oblique muscles. *Arch Ophthalmol.* 1946;36:661–673.
4. Scott WE, Kraft SP. Classification and treatment of superior oblique palsies: II. Bilateral superior oblique palsies. In: Caldwell D, ed. *Pediatric Ophthalmology and Strabismus: Transactions of the New Orleans Academy of Ophthalmology*. New York: Raven Press; 1986:265–291.
5. Scott WE, Parks MM. Differential diagnosis of vertical muscle palsies. In: von Noorden GK, ed. *Symposium on Strabismus: Transactions of the New Orleans Academy of Ophthalmology.* St. Louis: Mosby; 1978:118–134.
6. Straumann D, Steffen H, Landau K, et al. Primary position and Listing's law in acquired and congenital trochlear nerve palsy. *Invest Ophthalmol Vis Sci.* 2003;44:4282–4292.
7. Kushner BJ. Ocular torsion: rotations around the "WHY" axis. *J AAPOS.* 2004;8:1–12.
8. Kushner BJ. The diagnosis and treatment of bilateral masked superior oblique palsy. *Am J Ophthalmol.* 1988;105:186–194.
9. Graf M, Krzizok T, Kaufmann H. Das Kopfneigephanomen bei einseitigen und beidseitig symmetrischen Trochlearisparesen [Head-tilt test in unilateral and symmetric bilateral acquired trochlear nerve palsy.] *Klin Monatsbl Augenheilkd.* 2005;222:142–149.
10. Robinson DA. Bielschowsky head-tilt test: II. Quantitative mechanics of the Bielschowsky head-tilt test. *Vision Res.* 1985;25:1983–1988.
11. Simonsz HJ, Crone RA, van der Meer J, Merckel-Timmer CF, van Mourik-Noordenbos AM. Bielschowsky head-tilt test I: ocular coun-

terrolling and Bielschowsky head-tilt test in 23 cases of superior oblique palsy. *Vision Res.* 1985;25:1977–1982.
12. Demer JL, Miller JM. Magnetic resonance imaging of the functional anatomy of the superior oblique muscle. *Invest Ophthalmol Vis Sci.* 1995;36:906–913.
13. Chan TK, Demer JL. Clinical features of congenital absence of the superior oblique muscle as demonstrated by orbital imaging. *J AAPOS.* 1999;3:143–150.
14. Velez FG, Clark RA, Demer JL. Facial asymmetry in superior oblique palsy and pulley heterotopy. *J AAPOS.* 2000;4:233–239.
15. Kono R, Demer JL. Magnetic resonance imaging of the functional anatomy of the inferior oblique muscle in superior oblique palsy. *Ophthalmology.* 2003;110:1219–1229.
16. Demer JL, Miller MJ, Koo EY, Rosenbaum AL, Bateman JB. True versus masquerading superior oblique palsies: muscle mechanisms revealed by magnetic resonance imaging. In: Lennerstrand G, ed. *Update on Strabismus and Pediatric Ophthalmology*. Boca Raton, FL: CRC Press; 1995:303–306.
17. Kushner BJ. Errors in the three-step test in the diagnosis of vertical strabismus. *Ophthalmology.* 1987;96:127–132.
18. Brodsky ME. Three dimensions of skew deviation. *Br J Ophthalmol.* 2003;87:1440–1441.
19. Donahue SP, Lavin PJ, Hamed LM. Tonic ocular tilt reaction simulating a superior oblique palsy: diagnostic confusion with the 3-step test. *Arch Ophthalmol.* 1999;117:347–352.
20. Clark RA, Miller JM, Rosenbaum AL, Demer JL. Heterotopic muscle pulleys or oblique muscle dysfunction? *J AAPOS.* 1998;2:17–25.
21. Clark RA, Miller JM, Demer JL. Displacement of the medial rectus pulley in superior oblique palsy. *Invest Ophthalmol Vis Sci.* 1998; 39:207–212.
22. Shan X, Tian J, Ying HS, et al. Acute superior oblique palsy in monkeys, I: changes in static eye alignment. *Invest Ophthalmol Vis Sci.* 2007;48:2602–2611.
23. Shan X, Ying H, Tian J, et al. Acute superior oblique palsy in monkeys, II: changes in dynamic properties during vertical saccades. *Invest Ophthalmol Vis Sci.* 2007;48:2612–2620.
24. Tian J, Shan X, Ying HS, Walker MF, Tamargo RJ, Zee DS. The effect of acute superior oblique palsy on vertical pursuit in monkeys. *Invest Ophthalmol Vis Sci.* 2008;49:3927–3932.
25. Shan X, Tian J, Ying HS, et al. The effect of acute superior oblique palsy on torsional optokinetic nystagmus in monkeys. *Invest Ophthalmol Vis Sci.* 2008;49:1421–1428.
26. Tian J, Shan X, Zee DS, et al. Acute superior oblique palsy in monkeys, III: relationship to Listing's law. *Invest Ophthalmol Vis Sci.* 2007;48:2621–2625.
27. Quaia C, Shan X, Tian J, et al. Acute superior oblique palsy in the monkey: effects of viewing conditions on ocular alignment and modeling of the ocular motor plant. *Prog Brain Res.* 2008;171: 47–52.
28. Demer JL, Oh SY, Poukens V. Evidence for active control of rectus extraocular muscle pulleys. *Invest Ophthalmol Vis Sci.* 2000;41: 1280–1290.
29. Kono R, Poukens V, Demer JL. Quantitative analysis of the structure of the human extraocular muscle pulley system. *Invest Ophthalmol Vis Sci.* 2002;43:2923–2932.
30. Kono R, Poukens V, Demer JL. Superior oblique muscle layers in monkeys and humans. *Invest Ophthalmol Vis Sci.* 2005;46:2790–2799.
31. Miller JM, Demer JL, Poukens V, Pavlowski DS, Nguyen HN, Rossi EA. Extraocular connective tissue architecture. *J Vision.* 2003;3: 240–251.
32. Sheehan DC, Hrapchak BB. *Theory and Practice of Histotechnology.* St. Louis: Mosby; 1973.
33. Asmussen G, Kiessling A. Hypertrophy and atrophy of mammalian extraocular muscle fibres following denervation. *Experientia.* 1975;31:1186–1187.
34. Asmussen G, Kiessling A. Kaliberveranderungen der Muskelfasertypen des Musculus obliquus inferior Oculi des Kaninchens nach Denervierung. *Acta Anat (Basel).* 1976;96:386–403.
35. Asmussen G, Gaunitz U. Changes in mechanical properties of the inferior oblique muscle of the rabbit after denervation. *Pflugers Arch.* 1981;392:198–205.
36. Porter JD, Burns LA, McMahon EJ. Denervation of primate extraocular muscle: a unique pattern of structural alterations. *Invest Ophthalmol Vis Sci.* 1989;30:1894–1908.
37. Baker RS, Millett AJ, Young AB, Markesbery WR. Effects of chronic denervation on the histology of canine extraocular muscle. *Invest Ophthalmol Vis Sci.* 1982;22:701–705.
38. Christiansen SP, Baker S, Madhat M, Terrell B. Type-specific changes in fiber morphometry following denervation of canine extraocular muscle. *Exp Mol Pathol.* 1992;56:87–95.
39. Harrison AR, Anderson BC, Thompson LV, McLoon LK. Myofiber length and three-dimensional localization of NMJs in normal and botulinum toxin treated adult extraocular muscles. *Invest Ophthalmol Vis Sci.* 2007;48:3594–3601.
40. Goldberg SJ, Meredith MA, Shall MS. Extraocular motor unit and whole-muscle responses in the lateral rectus muscle of the squirrel monkey. *J Neurosci.* 1998;18:10629–10639.
41. Goldberg SJ, Wilson KE, Shall MS. Summation of extraocular motor unit tensions in the lateral rectus muscle of the cat. *Muscle Nerve.* 1997;20:1229–1235.
42. Tarkhan AA. The innervation of the extrinsic ocular muscles. *J Anat.* 1934;68:293–313.
43. Cheng-Minoda K, Ozawa T, Breinin GM. Ultrastructural changes in rabbit extraocular muscles after oculomotor nerve section. *Invest Ophthalmol Vis Sci.* 1968;7:599–616.
44. Velez FG, Isobe J, Zealear D, et al. Toward an implantable functional electrical stimulation device to correct strabismus. *J AAPOS.* 2009;13:229–235.
45. Jiang L, Demer JL. Magnetic resonance imaging of the functional anatomy of the inferior rectus muscle in superior oblique muscle palsy. *Ophthalmology.* 2008;115:2079–2086.
46. Kono R, Okanobu H, Ohtsuki H, Demer JL. Absence of relationship between oblique muscle size and Bielschowsky head tilt phenomenon in clinically diagnosed superior oblique palsy. *Invest Ophthalmol Vis Sci.* 2009;50:175–179.
47. Graf M, Weihs J. Effect of diagnostic occlusion in acquired trochlear nerve palsy. *Graefes Arch Clin Exp Ophthalmol.* 2009;247: 253–259.
48. Peng M, Demer JL. Functional implications of compartmentalized innervation of the lateral rectus muscle. *Soc Neurosci Abstr.* 2009: 356.8.
49. Buttner-Ennever JA, Eberhorn A, Horn AKE. Motor and sensory innervation of extraocular eye muscles. *Ann N Y Acad Sci.* 2003; 1004:40–49.
50. Kashii S, Matsui Y, Honda Y, Ito J, Sasa M, Takaori S. The role of extraocular proprioception in vestibulo-ocular reflex of rabbits. *Invest Ophthalmol Vis Sci.* 1989;30:2258–2264.
51. Demer JL, Ortube MC, Engle EC, Thacker N. High resolution magnetic resonance imaging demonstrates abnormalities of motor nerves and extraocular muscles in patients with neuropathic strabismus. *J AAPOS.* 2006;10:135–142.
52. Shokida F, Eleta M, Gabriel J, Sanchez C, Seclen F. Superior oblique muscle MRI asymmetry and vertical deviation in patients with unilateral superior oblique palsy. *Binocul Vis Strabismus Q.* 2006; 137–146.
53. Demer JL. A 12 year, prospective study of extraocular muscle imaging in complex strabismus. *J AAPOS.* 2003;6:337–47.
54. Ozkan S, Aribal ME, Sener EC, Sanac AS, Gurcan F. Magnetic resonance imaging in evaluation of congenital and acquired superior oblique palsy. *J Pediatr Ophthalmol Strabismus.* 1997;34:29–34.
55. Horton JC, Tsai RK, Truwit CL, Hoyt WF. Magnetic resonance imaging of superior oblique muscle atrophy in acquired trochlear nerve palsy (letter). *Am J Ophthalmol.* 1990;110:315–316.
56. Sato M. Magnetic resonance imaging and tendon anomaly associated with congenital superior oblique palsy. *Am J Ophthalmol.* 1999;127:379–387.
57. Sato M, Yagasaki T, Kora T, Awaya S. Comparison of the muscle volume between congenital and acquired superior oblique palsies by magnetic resonance imaging. *Jpn J Ophthalmol.* 1998;42:466–470.
58. Saunders RA. When and how to strengthen the superior oblique muscle. *J AAPOS.* 2009;13:430–437.
59. Miller JM, Pavlovski DS, Shaemeva I. Orbit 1.8. *Gaze Mechanics Simulation*. San Francisco: Eidactics; 1999.